Dalton Transactions

ROYAL SOCIETY OF CHEMISTRY

PAPER

View Article Online
View Journal | View Issue

Cite this: *Dalton Trans.*, 2022, **51**, 6014

Application of the anthraquinone drug rhein as an axial ligand in bifunctional Pt(IV) complexes to obtain antiproliferative agents against human glioblastoma cells†

Elisabetta Gabano, ‡[a] Marzia Bruna Gariboldi,‡[b] Giulia Caron, [c] Giuseppe Ermondi,[c] Emanuela Marras,[b] Maura Vallaro[c] and Mauro Ravera *[a]

Received 24th January 2022,
Accepted 18th March 2022

DOI: 10.1039/d2dt00235c

rsc.li/dalton

Octahedral Pt(IV) prodrugs are an effective way to combine cisplatin-like moieties and a second drug to obtain selective and stimuli responsive bifunctional antiproliferative compounds. Recently, two bifunctional Pt(IV) complexes have shown interesting *in vitro* and *in vivo* effects in glioblastoma, the most aggressive primary brain tumor. An interesting observation indicates that 4,5-dihydroxy-9,10-dioxo-9,10-dihydroanthracene-2-carboxylic acid (**rhein**) can inhibit *in vivo* glioma tumor progression. Furthermore, a prodrug in which cisplatin was combined with two molecules of **rhein** showed a potency higher than that of cisplatin toward cisplatin-resistant lung carcinoma cells. However, the high lipophilicity of this type of complex affects their solubility and bioavailability. To overcome these limits, in the present work, three Pt(IV) derivatives were obtained by differently linking one molecule of **rhein** and one acetato ligand at the axial position to a cisplatin core. The complexes proved to be similar to or more potent than the parent cisplatin and **rhein**, and the reference drug temozolomide on two human glioblastoma cell lines (U87-MG and T98G). They retained their activity under hypoxia and caused a significant reduction in the motility of both cell lines, which can be related to their ability to inhibit MMP2 and MMP9 matrix metalloproteinases. Finally, physicochemical and computational studies indicated that these Pt(IV) derivatives are more prone than **rhein** to cross the blood–brain barrier.

Introduction

Malignant gliomas are the most common tumors of the central nervous system (about 6 cases per 100 000 people are diagnosed worldwide every year),[1] with glioblastoma multiforme (GBM) accounting for about 60% of all gliomas (*i.e.*, 3.5 cases per 100 000 people in developed countries).[2] The adjective *multiforme* (multifaceted) indicates the inter- and intra-tumor heterogeneity that is present in this kind of glioma, as well as hypermutation that appears as a consequence of chemotherapy. This mutability explains why these tumors are sadly associated with a dismal prognosis and poor quality of life, and remain difficult to treat, although therapeutic options have been improved in the last few years.[3] The disease course is rapid and overall estimates of survival among patients with GBM are 25% patients alive 2 years after diagnosis and only 5–10% of patients alive at 5 years.[4]

The current standard treatment of GBM includes surgery, followed by radio- and concurrent chemo-therapy with the oral alkylating agent temozolomide (**TMZ**). With this therapeutic protocol, a little progress in median overall survival from approx. 7 months to 17 months was observed.[4] Understandably, the extensive surgical resection of GBM is difficult because of its location. Moreover, infiltrating tumor cells remain invariably within the surrounding tissue, leading to inadequate recovery and recurrence of the disease.[5] Since the cures for GBM are not always effective, new strategies are needed to overcome the resistance to standard therapeutic treatments.[6]

Naturally occurring **rhein** (4,5-dihydroxy-9,10-dioxo-9,10-dihydroanthracene-2-carboxylic acid or cassic acid, Fig. 1) has

[a]*Dipartimento di Scienze e Innovazione Tecnologica, Università del Piemonte Orientale, Viale Michel 11, 15121 Alessandria, Italy.*
E-mail: mauro.ravera@uniupo.it
[b]*Dipartimento di Biotecnologie e Scienze della Vita (DBSV), Università dell'Insubria, via Dunant 3, Varese, Italy*
[c]*CASSMedChem, Dipartimento di Biotecnologie Molecolari e Scienze per la Salute, Università di Torino, Via Quarello 15, 10135 Torino, Italy*

†Electronic supplementary information (ESI) available: ESI-MS, ^{1}H, ^{13}C, ^{195}Pt, [^{1}H, ^{1}H] COSY and [^{1}H, ^{13}C] HSQC NMR spectra of complexes **1–3**; solution behavior of **1–3**; ESI-MS spectra of ^{15}N-labeled **1–3**; [^{1}H, ^{15}N] HSQC NMR spectra of ^{15}N-**1–3** before and after reduction with cytosol. See DOI: https://doi.org/10.1039/d2dt00235c

‡These authors contributed equally.

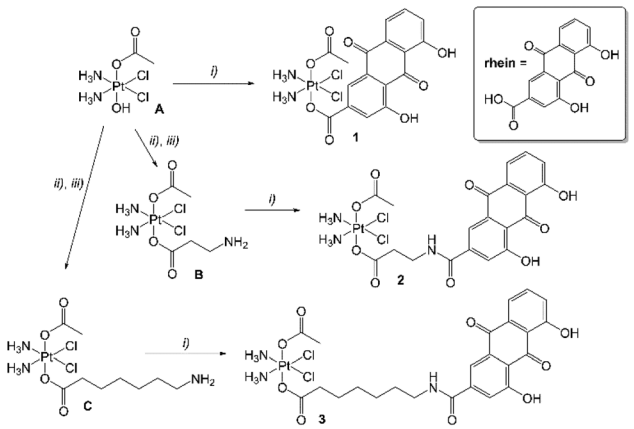

Fig. 1 Synthesis of the complexes under investigation: (i) **rhein**, HATU and DIPEA; (ii) Fmoc-β-alanine or 7-(Fmoc-amino)heptanoic acid, HATU and DIPEA; (iii) piperidine. Fmoc = 9-fluorenylmethoxycarbonyl group; HATU = 1-[bis(dimethylamino)methylene]-1*H*-1,2,3-triazolo[4,5-*b*]pyridinium 3-oxide hexafluorophosphate; DIPEA = *N*,*N*-diisopropylethylamine.

a number of pharmacological effects (*e.g.*, anti-inflammatory, anti-fibrosis, and anti-oxidant activity),[7] and it exerts anticancer effects by modulating cellular proliferation, apoptosis, migration, and invasion.[8–10] Interestingly, nasal administration of the potassium salt of **rhein** appreciably inhibited tumor progression in mice intracranially injected with GL261 glioma cells.[11] This result was associated with the inhibitory effect of **rhein** on the ectoenzyme CD38, which has several functions as both a nicotinamide adenine dinucleotide glycohydrolase and a cell surface receptor, and its deficiency was correlated with increased cell death in the tumor mass.[12,13]

It is now well known that cancer is a multifactorial disease and combination therapy, using two or more therapeutic agents, may target several key pathways in an additive or a synergistic way, enhancing the treatment's efficacy. Thus, two drugs or two pharmacophores with complementary action can be combined in a single molecule, obtaining a "bifunctional drug" able to elicit two different primary pharmacological actions. For example, **rhein** was successfully combined with the histone deacetylase inhibitor suberoylanilide hydroxamic acid (SAHA) in a **rhein**–SAHA hybrid that was more effective than **rhein** and SAHA alone in the inhibition, proliferation, invasion and migration of glioma cells.[14]

Nevertheless, the bifunctional drug can be designed for the concurrent delivery and release of the two moieties. One of these moieties can be represented by cisplatin ($[PtCl_2(NH_3)_2]$, (*SP*-4-2)-diamminedichloridoplatinum(II), **CDDP**), a well-known antitumor agent that is clinically used against a wide variety of solid tumors. An effective way to combine **CDDP**-like moieties and a second drug may be represented by the octahedral Pt(IV) complexes. They comprise a class of compounds that are particularly well suited to obtain selective and stimuli responsive bifunctional compounds, due to their ability to act as prodrugs. In fact, they should be designed to be specifically reduced in the hypoxic tumor tissue, to give the cytotoxic Pt(II) metabolite with the concomitant loss of the two axial ligands (activation by reduction).[15–21] In this regard, two bifunctional Pt(IV) complexes, containing 2-(2-propynyl)octanoate and a methyltetrahydropyridin derivative, respectively, were reported to be effective against GBM in both *in vitro*[22–24] and *in vivo*[25] models. In addition, a recent review discussed the anticancer effects and advantages of platinum-based drugs in the field of brain tumors.[26]

In this context, **CDDP** has been combined with two molecules of **rhein** to obtain a prodrug that showed a potency higher than that of cisplatin toward lung carcinoma cells (A549 and cisplatin resistant A549/DDP subline) and higher antitumor efficacy in the A549/DDP xenograft model.[27] However, Pt(IV) complexes with two very lipophilic axial ligands, such as **rhein**, usually suffer from low solubility and limited bioavailability. Therefore, we synthesized three different Pt(IV) compounds in which one molecule of **rhein** was linked in different ways at the axial position to a **CDDP** core. The coordination geometry was completed by a hydrophilic acetato ligand. The resulting complexes **1–3** (Fig. 1) were then tested on two human GBM cell lines to evaluate their effects on cell viability and on migration. Moreover, the estimated ability of **1–3** to cross the blood–brain barrier was also studied.

Results and discussion

Synthesis and solution properties of the Pt(IV) complexes 1–3

The investigated complexes were designed to link one molecule of **rhein** in two different ways, either directly or through a spacer of two lengths (Fig. 1). The common starting molecule was (*OC*-6-44)-acetatodiamminedichloridohydroxidoplatinum (IV), **A**, obtained by oxidizing **CDDP** with hydrogen peroxide in acetic acid.[28] In the case of complex **1**, **rhein** was directly reacted with **A**, upon its activation with the coupling agent HATU (1-[bis(dimethylamino)methylene]-1*H*-1,2,3-triazolo[4,5-*b*]pyridinium 3-oxide hexafluorophosphate) in the presence of DIPEA (*N*,*N*-diisopropylethylamine). In the case of complexes **2** and **3**, intermediate **A** was firstly converted into the corresponding intermediates **B** and **C** upon reaction with Fmoc-β-alanine and 7-(Fmoc-amino)heptanoic acid, respectively, and following deprotection with piperidine[29] (Fmoc = 9-fluorenylmethoxycarbonyl group). Finally, **rhein**, activated with HATU and DIPEA, was reacted with complexes **B** and **C**, to obtain **2** and **3**, respectively.

Complexes **1–3** were challenged with cell culture medium to investigate their behavior in solution by following the RP-HPLC peak of the compounds over 72 h, the time used in the cytotoxicity tests (see the ESI, Fig. S20†). All the complexes proved to be not completely stable, as the original peaks disappeared within 72 h, with the formation of hydrolyzed species. This behavior was observed for several other Pt(IV) compounds, undermining the paradigm that Pt(IV) is kineti-

cally stable.[30–32] However, the conversion of the complexes in cell culture medium is limited in the first hours and does not affect the overall accumulation and final effect of the prodrugs, which is ruled by the fast reduction of the complexes within the cells.[33,34]

The latter hypothesis was checked by studying the reduction of complexes **1–3** by means of [^{1}H, ^{15}N] HSQC (Heteronuclear Single Quantum Coherence) NMR spectroscopy. The ^{15}N-labeled **1–3** were prepared by using [$PtCl_2(^{15}NH_3)_2$] as the starting material,[35] and challenged with the cytosolic extract of A2780 ovarian cancer cells as a model. After 2 h of reaction, the spectra showed only the signal of ^{15}N-**CDDP** (^{15}N δ = −66.9 ppm; ^{1}H δ = 3.99 ppm) confirming the expected fast activation by reduction mechanism mediated by the cytosolic content (see the ESI, Fig. S24–S29†).[36–39]

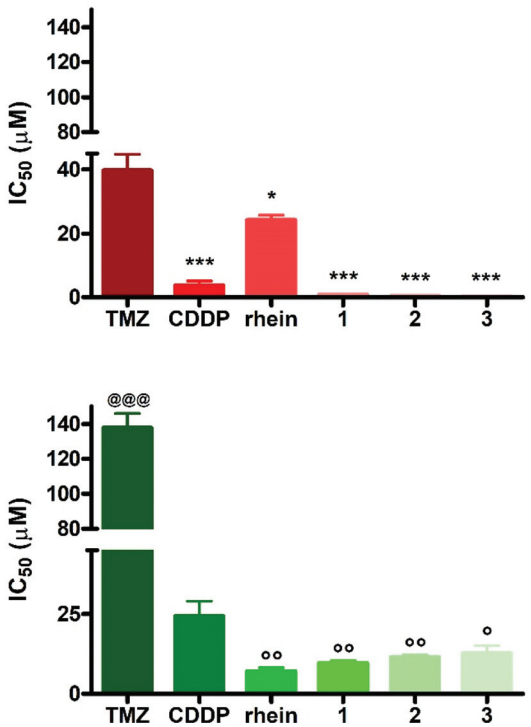

Fig. 2 IC_{50} values obtained by MTT assay in (top) U87-MG and (bottom) T98G cells following 72 h treatment with **rhein** and its Pt(IV) derivatives **1–3**. TMZ and **CDDP** were used as reference compounds. Data are mean ± standard deviation (sd) of six independent experiments; *p < 0.05 *vs.* TMZ; ***p < 0.001 *vs.* TMZ and **rhein**; *p < 0.05 *vs.* TMZ; $^{@@@}p$ < 0.001 *vs.* all the others; °°p < 0.01 *vs.* **CDDP**; °p < 0.05 *vs.* **CDDP**.

Effects on cell viability

The effect of the complexes **1–3** on cell viability was determined on the two human GBM cell lines T98G and U87-MG. Tumor cells were incubated with the compounds for 72 h, and MTT (3-(4,5-dimethylthiazol-2-yl)-2,5-diphenyltetrazolium bromide) reduction assay was used to detect viable cells. The results were expressed as the half inhibitory concentration, IC_{50}, and compared to those obtained after treatment of the cells with the reference compounds temozolomide (TMZ), **rhein** and **CDDP** (Fig. 2 and Table 1).

Fig. 2 shows at a glance that both cell lines were significantly more sensitive to all Pt complexes and **rhein** than TMZ, with IC_{50} ratios [IC_{50}(TMZ)/IC_{50}(Pt(IV) or **rhein**)] ranging from 1.6 (**rhein**) to 102 (**3**) on U87-MG, and from 5.6 (**CDDP**) to 19.5 (**rhein**) on T98G. Furthermore, T98G cells were less sensitive than U87-MG to Pt(IV) derivatives and to TMZ. This latter result agrees with the data reported by other authors.[40] In general, the p53 status has been correlated with drug resistance in many tumors.[41] Furthermore, a correlation between the p53 gene status and cisplatin response was reported, with the greatest response observed in p53 wild-type tumors and a relatively lower response rate observed in p53 mutated tumors.[42] Thus, the different response of the two cell lines to reference compounds and Pt(IV) derivatives can be, at least in part, explained considering that U87-MG cells carry a wild-type form, while T98G is a mutated form, of p53.[43,44]

Interestingly, in the T98G cell line, **rhein** showed similar efficacy to the Pt derivatives, whereas in U87-MG cells, **1**, **2** and **3** were significantly more potent than the organic compound.

Effect on cell migration

As already mentioned in the Introduction, aggressive invasiveness is a common feature of GBM.[45–47] Although cell migration is required for physiological functions, cancer cell motility and invasion are among the crucial, though not sufficient, hallmarks of metastasis development.[48]

With that in mind, the effect of **CDDP**, **rhein** and **1–3** derivatives on cellular migration was assessed using the

Table 1 Half maximal inhibitory concentration (IC_{50}, μM) obtained by MTT assay in U87-MG and T98G cells following 72 h treatment with TMZ, **rhein** and **1–3** derivatives under normoxia (72 h, O_2 21%) or hypoxia (24 h, O_2 21% and 48 h, O_2 1%). Data are mean ± SD of six independent experiments; *p < 0.05 *vs.* TMZ; ***p < 0.001 *vs.* TMZ and **rhein**;$^{§}p$ < 0.05 *vs.* **rhein**; $^{\#}p$ < 0.01 *vs.* normoxia

	Normoxia		Hypoxia	
Compound	U87-MG	T98G	U87-MG	T98G
TMZ	39.72 ± 5.17	137.85 ± 20.14	17.10 ± 1.50$^{\#}$	148.92 ± 30.73$^{\#}$
CDDP	3.70 ± 1.17***	24.30 ± 4.37***	2.73 ± 0.09***	19.85 ± 1.88***
rhein	24.19 ± 3.74*	7.08 ± 2.34***	24.93 ± 0.64*	61.73 ± 2.33***,$^{\#}$
1	0.87 ± 0.19***	9.62 ± 1.13***	1.20 ± 0.21***	12.40 ± 0.17***,§
2	0.49 ± 0.14***	11.40 ± 1.37***	0.54 ± 0.07***	13.01 ± 0.86***,§
3	0.38 ± 0.08***	12.65 ± 1.17***	0.43 ± 0.03***	15.81 ± 1.28***,§

scratch wound healing assay. This is a simple and low-cost method to evaluate cellular migration in 2D models and to study *in vitro* the anti- or pro-migration effects of a variety of experimental conditions and drugs.[49–51] Briefly, in this assay, a cell-free area (wound gap) is physically created in a confluent monolayer of cells by scratching. The healing of the gap by migration and growth of the cells towards the center of the gap is monitored, quantified, and expressed as the percentage of closure of the "wounded" area with time. Cell motility or growth alterations or both can lead to a modified rate of closure of the gap.[52]

U87-MG and T98G cells have been shown to possess intrinsic migratory capacity;[53–55] thus, the effect of a subtoxic concentration of the compounds, corresponding to the respective IC_{20} values, on the migration of the cells was evaluated on both cell lines. Images of the wounded area were acquired immediately after the production of the scratch and 24 h later through a camera connected to an inverted microscope (Fig. 3).

To better represent scratch wound healing results, percentages of the open scratch wound detected after 24 h were normalized *vs.* the same percentage at 0 h and are shown in Fig. 4. In general, in the absence of treatment, U87-MG cells migrated faster than T98G cells, as indicated by the smaller uncovered surface at 24 h, Fig. 3. As shown in the same figure, in both cell lines, **CDDP** treatment unveiled similar results to the controls. In the literature, an antimigratory effect of **CDDP** has been reported in ovarian cell lines; however, **CDDP** concentrations used in that study were higher than those used in the present one to achieve subtoxic effects.[56]

Different authors reported that **rhein** exerted inhibitory effects on migration in several cancer cell lines, including T98G cells.[14,57,58] In agreement, a significant inhibition of T98G cell migration, compared to controls, was observed in the present work following exposure at a concentration that affects cell viability only minimally. In U87-MG cells, under the same conditions, only a slight increase in the % of open wound was observed.

Concerning the Pt(IV) derivatives, a significant reduction in cell motility was observed following treatment with subtoxic concentrations of **1–3** in both cell lines. In particular, complexes **3** (in U87-MG cells) and **1** (in T98G cells) were signifi-

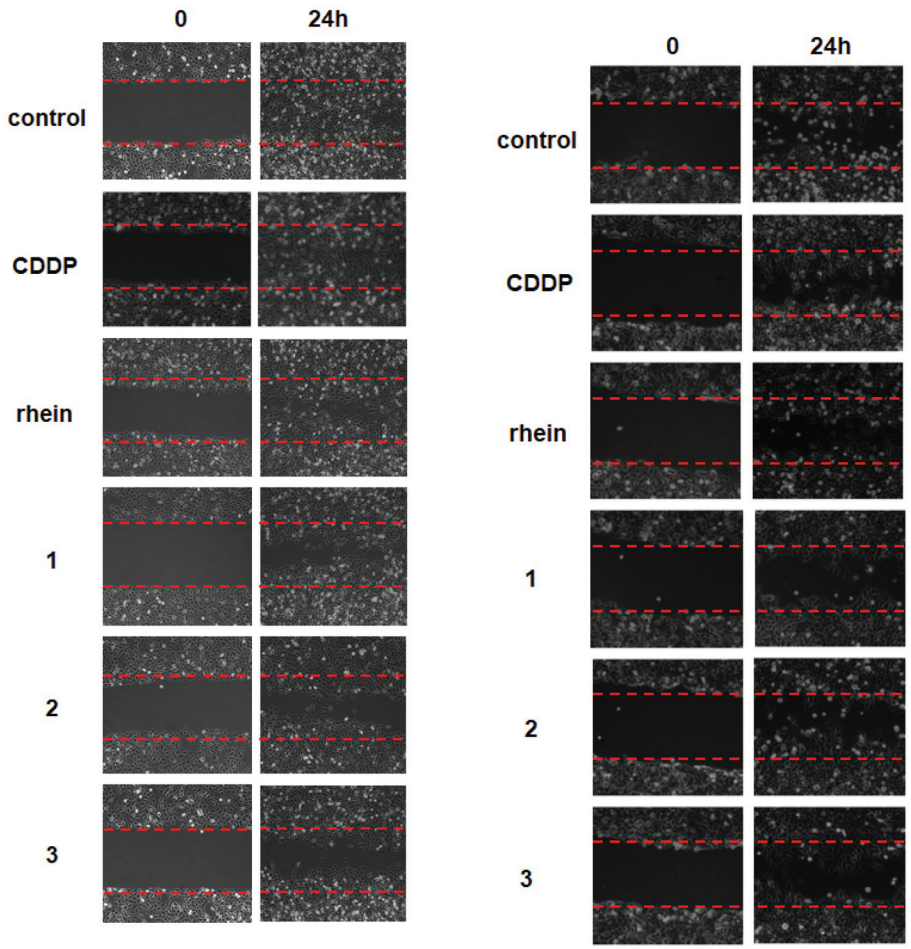

Fig. 3 Migratory activity of (left column) U87-MG and (right column) T98G cells following treatment with subtoxic concentrations (IC_{20}) of **rhein**, **CDDP** and **1–3** derivatives. Pictures of the scratch wound were taken immediately after the production of the scratch (0) and 24 h later.

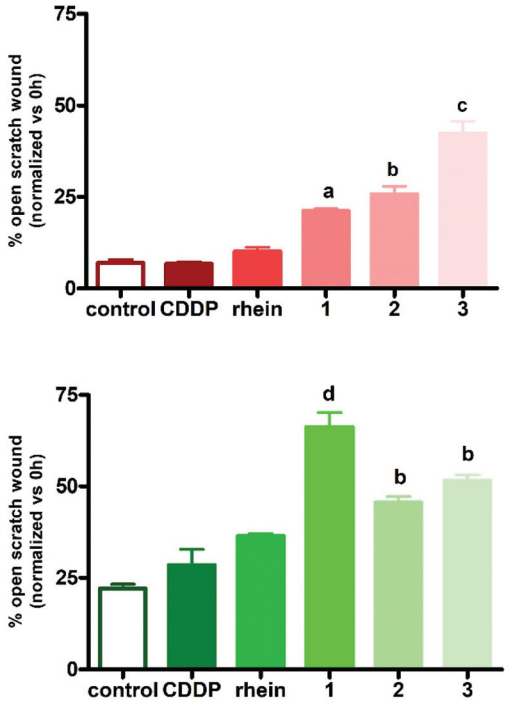

Fig. 4 Percentage of open scratch wound, normalized *vs.* 0 h, in (top) U87-MG and (bottom) T98G cells following 24 h incubation with sub-toxic concentrations (IC_{20}) of **rhein**, **CDDP** and **1–3** derivatives. Data are mean ± SD of three independent experiments; *$p < 0.05$ *vs.* control; (a) $p < 0.05$ *vs.* control, **CDDP**, and **rhein**; (b) $p < 0.05$ *vs.* control, **CDDP**, and **rhein**; (c) $p < 0.001$ *vs.* control, **CDDP**, and **rhein** and $p < 0.01$ *vs.* **1** and **2**; (d) $p < 0.01$ *vs.* control, **CDDP**, and **rhein** and $p < 0.05$ *vs.* **2** and **3**.

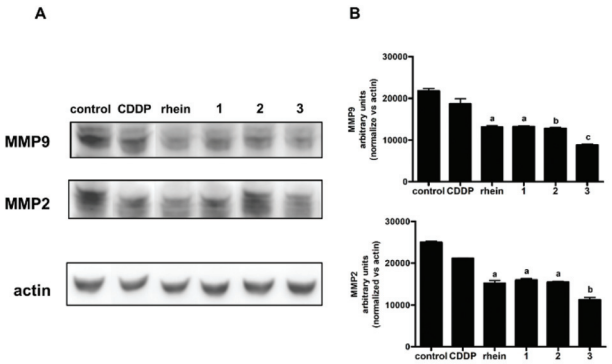

Fig. 5 (A) MMP9 and MMP2 protein levels and (B) densitometric analysis in U87-MG cells treated 72 h with **CDDP**, **rhein** and **1–3** derivatives at concentrations corresponding to the respective IC_{20}. (A) Images of a representative experiment out of three independent experiments with similar results; (B) Results of all the experiments performed, that were normalized *vs.* actin protein levels ((a) $p < 0.01$ *vs.* control and **CDDP**; (b) $p < 0.001$ *vs.* control and **CDDP** and $p < 0.05$ *vs.* **1** and **2**).

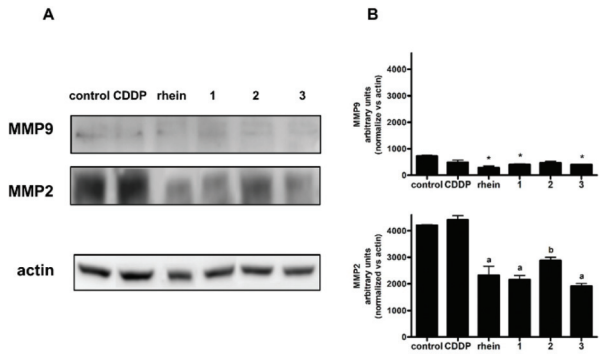

Fig. 6 (A) MMP-9 and MMP-2 protein levels and (B) densitometric analysis in T98G cells treated 72 h with **CDDP**, **rhein** and **1–3** derivatives at concentrations corresponding to the respective IC_{20}. (A) Images of a representative experiment out of three independent experiments with similar results; (B) Results of all the experiments performed, that were normalized *vs.* actin protein levels (*$p < 0.05$ *vs.* control; (a) $p < 0.01$ *vs.* control and **CDDP**; (b) $p < 0.05$ *vs.* control and **CDDP**).

cantly more potent than all the other compounds in reducing cell migration (Fig. 4).

Extracellular matrix (ECM, the macromolecular network that constitutes the scaffold of tissues and organs) and basal membrane degradation is the first step for cancer cell migration and invasion. For maintaining normal tissue architecture and functions, the balance between ECM destruction and deposition is important. This is modulated by matrix metalloproteinases (MMPs, a family of enzymes whose activity is directed against the components of the ECM) and their tissue inhibitors. The high expression of different MMPs, including MMP-1, -2, -3, -7, -9, -13, -14, facilitates tumor cell invasion and metastasis.[59] In particular, MMP2 (gelatinase-A) and MMP9 (gelatinase-B) are deeply associated with the presence of metastatic tumors.[60,61] In human gliomas, a strong correlation has been reported between high MMP levels (MMP2 and MMP9, in particular) and invasiveness.[62]

It has been previously reported that **rhein** significantly inhibited the migration of ovarian cancer cells by down regulating MMP1, MMP2 and MMP9 expression.[58,63] In agreement, the results in Fig. 5 and in Fig. 6 show that also in U87-MG and T98G GBM cell lines **rhein** was able to significantly down-regulate MMP2 and MMP9 protein levels. Furthermore, also equitoxic concentrations of **1**, **2** and **3** inhibited MMP2 and MMP9 to a similar extent, while no alterations in the levels of these proteins were observed following treatment with **CDDP** in both cell lines. Thus, the observed inhibitory effect on cellular migration exerted by **1**, **2** and **3** could be, at least in part, attributed to their inhibitory activity against MMP2 and MMP9.

Cell response in hypoxia

Hypoxia, defined as the decreased availability of oxygen, is one of the major features characterizing solid tumors. Hypoxic regions may serve as a niche for the maintenance of cancer stem cells,[64] and may induce large adaptive changes at the cellular level favoring tumor progression.[65–68] In particular, a hypoxic microenvironment is protective for glioblastoma, thus inducing cells to undergo malignant progression.[69] Furthermore, cancer hypoxia has been associated with resis-

tance to radio- and chemo-therapy, leading to an insufficient response to classic drug treatment.[70]

For this reason, the relative effect of hypoxia on the response of U87-MG and T98G cells to the compounds under investigation was evaluated by the MTT assay also under hypoxic conditions (O_2 1%, see the Experimental section). A comparison of the IC_{50} values obtained under normoxic and hypoxic conditions is reported in Table 1.

A number of experimental pieces of evidence suggest that the antiproliferative activity of **CDDP** is reduced under hypoxic conditions.[71–73] However, no significant differences in U87-MG and T98G response to **CDDP** under hypoxia, compared to normoxia, was observed. Regarding the other compounds, a similar ratio of activity, compared to references, was maintained in both cell lines either under hypoxia or normoxia. The only deviation was the result obtained with **rhein** in T98G cells; as a matter of fact, **rhein** was significantly more potent under normoxia than under hypoxia, thus changing the ratio.

A particularly intriguing result concerns compounds **1–3**, which under hypoxia retained their effects on cell viability, as observed for other Pt(IV) derivatives on different cancer cell lines.[39,74–79]

Physicochemical properties and estimation of blood–brain barrier crossing

The blood–brain barrier (BBB) is a specialized system of capillary endothelial cells that regulates ion trafficking, as well as the nutrient and oxygen supply.[80]

It prevents approximately 98% of small molecules (smaller than 500 Da) and nearly 100% of large molecules from entering the brain, thus strictly limiting therapeutic intervention by impeding the systemic delivery of chemotherapeutics and other molecular-targeting assemblies. Although the tumors are known to compromise the integrity of the BBB and to increase its permeability, it still contributes in hampering drug accumulation in brain tumors.[81]

Lipophilicity and ionization have been related to the ability of compounds to cross the BBB, although there is a general agreement in the literature that the main molecular property affecting drug BBB passage is the H-bonding potential (*i.e.*, the skill of a given molecule to form H bonds, HBs, with BBB components).[82] Therefore, the ionization, lipophilicity and H-bonding potential of the investigated compounds were determined in the work at this stage.

The ionization behavior of **rhein** was firstly assessed; MarvinSketch v. 20.19.0 predicted three acidic centers with the following pK_a values: 3.40 (COOH); 7.89 (OH close to COOH); 8.54 (OH distant from COOH). Although potentiometric titrations in water and in water/methanol mixtures were biased by solubility issues, one pK_a between 4 and 5, a second pK_a at 8.7 and a third pK_a above 12 were experimentally observed for **rhein**. Therefore, at pH = 7.0 **rhein** is largely in its anionic form. On the contrary, pK_a prediction could not be performed for **1–3**, since Pt(IV) is not parameterized in any software developed for pK_a calculations. However, potentiometric titrations showed an acidic pK_a = 8.1 for **1**. Derivatives **2** and **3** were largely insoluble in the whole pH range but structural considerations suggest that they share a similar ionization profile to **1**, thus they are expected to be neutral at pH = 7.0.

Table 2 Physicochemical data of investigated compounds

Cmpd	$\log D_{oct}$	$\log D_{tol}$	$\log k_w^{IAM}$	$\Delta\log D_{oct\text{-}tol}$	$\Delta\log k_w^{IAM}$
rhein	−0.27	<−2.5	1.62	>2.5	2.36
1	1.85	−0.85	2.50	2.7	1.51
2	1.02	−0.52	2.13	1.54	1.54
3	2.27	0.07	3.06	2.20	1.92

Rhein and Pt(IV) derivatives were then characterized for their lipophilicity in three systems at pH = 7.0 (Table 2). First, the lipophilicity in the reference system *n*-octanol/water ($\log D_{oct}$) was measured. The different ionization pattern supports the lower $\log D_{oct}$ of **rhein** (anion) when compared with the Pt(IV) derivatives (neutral). Similar results were obtained in the toluene/water system ($\log D_{tol}$). Notably, **3** is the most lipophilic Pt(IV) derivative in both biphasic systems whereas **1** is more lipophilic than **2** in *n*-octanol/water but not in toluene/water.

Finally, a chromatographic lipophilicity index in a biomimetic environment was measured ($\log k_w^{IAM}$, IAM standing for Immobilized Artificial Membrane. In IAM chromatographic columns, the covalent binding of a monolayer of phospholipids to silica particles permits to obtain a stationary phase able to mimic the lipid environment of a cell membrane).[83] IAM chromatography is sensible to the presence of charges, and this could explain the higher $\log k_w^{IAM}$ value of **rhein** compared to those of **1**, **2** (very close one with the other) and **3** (Table 2).

Two main experimental descriptors of the molecular HB potential have been reported in the literature and related to BBB permeability: $\Delta\log P_{oct\text{-}alk}$ and $\Delta\log k_w^{IAM}$. $\Delta\log P_{oct\text{-}alk}$ is the difference between the partition coefficients in the octanol/water and hydrocarbon/water systems. Young *et al.* in 1988 showed a highly significant correlation between $\Delta\log P_{oct\text{-}alk}$ and the logarithms of the brain/blood ratios (log BB) for 20 structurally different compounds involving twenty H2 antagonists.[84] In another study, the H-donor capability was also related to the CNS (central nervous system) entering potential of seven phenylalanine oligomers esterified with carboxylic moieties.[85,86]

$\Delta\log k_w^{IAM}$ can be obtained when experimental $\log D_{oct}$ and $\log k_w^{IAM}$ values are available; the higher the $\Delta\log k_w^{IAM}$, the more polar the compound.[87] Highly significant inverse linear relationships between $\Delta\log k_w^{IAM}$ and log BB values were observed in two works studying 14 structurally unrelated basic drugs and eight acidic compounds, respectively.[88,89]

In Table 2 $\Delta\log D_{oct\text{-}tol}$ and $\Delta\log k_w^{IAM}$ are reported. For **1–3**, but not for **rhein**, the partition coefficient *P* is equal to *D*, thus in this study we prefer to refer to $\Delta\log D$ rather than $\Delta\log P$. Moreover, to limit solubility issues in alkanes, toluene replaced alkanes and thus $\Delta\log D_{oct\text{-}tol}$ was measured instead of $\Delta\log D_{oct\text{-}alk}$, as suggested in a previous report.[90]

For interpretative purposes, it should be recalled that the higher the $\Delta\log D_{\text{oct-alk}}/\Delta\log k_{\text{w}}^{\text{IAM}}$, the more likely the compound forms HBs with BB components, the less prone it is to cross the BBB. Furthermore, the presence of intramolecular HBs (IMHBs) causes a decrease in $\Delta\log D_{\text{oct-alk}}/\Delta\log k_{\text{w}}^{\text{IAM}}$ values. $\Delta\log D_{\text{oct-tol}}$ and $\Delta\log k_{\text{w}}^{\text{IAM}}$ values in Table 2 indicate that **rhein** has a higher capacity to form HBs with BBB components than the Pt(IV) derivatives. This result is compatible with the formation of IMHBs that masks the polarity of the Pt(IV) amino groups. To explore the capacity of IMHB formation, Pt(IV) complexes and **rhein** were investigated with molecular modeling strategies. In particular, the compounds were subjected to a conformational sampling procedure and the resulting conformers were minimized using an implicit solvent treatment to mimic (a) the water (polar) environment and (b) the interior of membranes (nonpolar, see the Experimental section for details). The results are shown in Fig. 7 which shows that the amino ligands present in the three Pt(IV) complexes are involved in the formation of IMHBs with the carboxylic group in both the nonpolar and polar environments. Focusing only on minimum-energy conformers could leave doubts about the presence of IMHBs in the real biological environment, where the temperature and interaction with the solvent and membrane-forming molecules can provide the energy needed to break IMHBs. The persistence of IMHBs in conformers with a higher energy than the lowest energy conformer shown in Fig. 7 strengthens the hypothesis that the three complexes can form IMHBs even in a real environment.

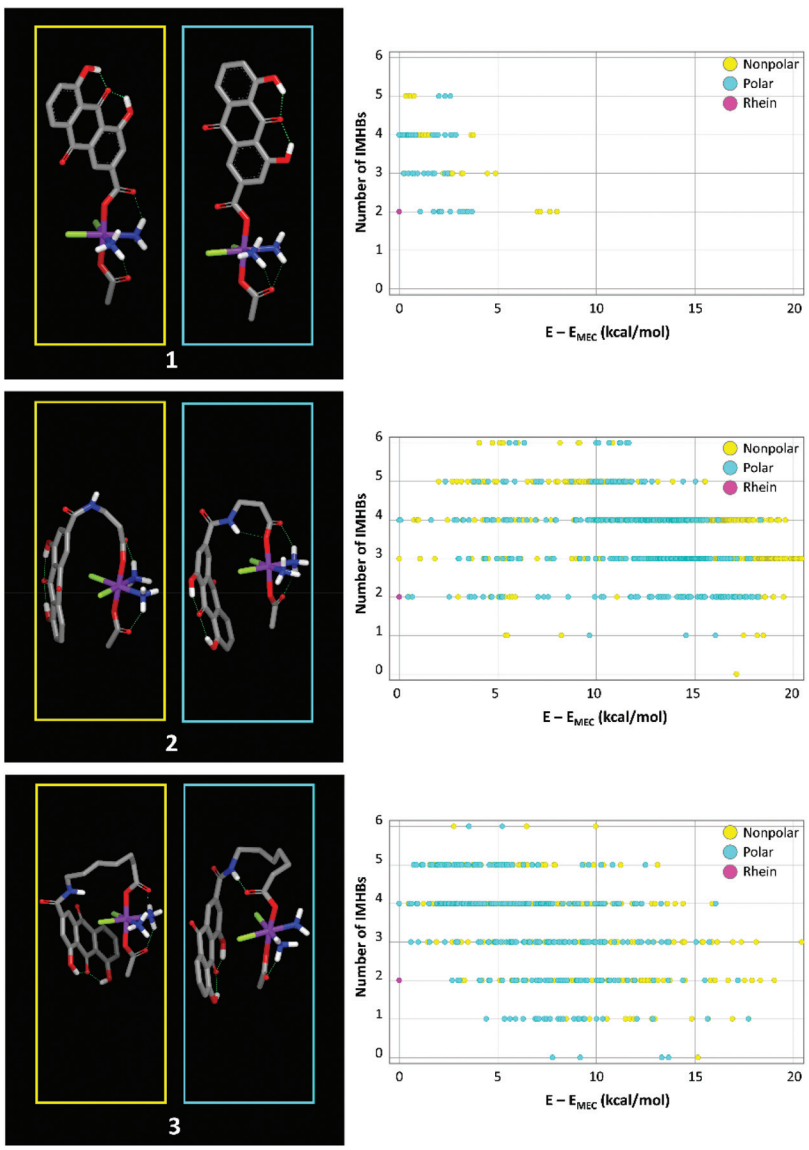

Fig. 7 For each Pt(IV) derivative reported, from the left to the right side: the minimum energy conformer (MECs) in (i) a nonpolar environment (yellow rectangle) and (ii) in a polar environment (blue rectangle); (iii) the number of IMHBs *vs.* the difference of energy of the conformer respect to the MEC ($E - E_{\text{MEC}}$) graph. In each plot yellow and cyan bullets refer to conformers present in nonpolar and polar environments, respectively. Pink bullet refers to **rhein**.

In particular, the energy-weighted average number of IMHBs of the three complexes ranges from 3.2 to 4.1 in the nonpolar environment and from 3.4 to 4.1 in the polar environment. These results are consistent with the presence of the above-said network of IMHBs.

Overall, the physicochemical analysis combined with the computational study supports that Pt(IV) derivatives are more prone to cross the BBB than **rhein**.

Experimental section

General procedures

4,5-Dihydroxy-9,10-dioxo-9,10-dihydroanthracene-2-carboxylic acid (**rhein**, Tokyo Chemical Industry) and all the other chemicals (Alfa Aesar-Thermo Fisher Scientific or Sigma Aldrich-Merck, except where otherwise specified) were used as received. Complexes (*SP*-4-2)-diamminedichloridoplatinum(II) (cisplatin),[91] (*OC*-6-44)-acetatodiamminedichloridohydroxidoplatinum(IV), **A**,[28,92] (*OC*-6-44)-acetato(β-alaninato)diamminedichloridoplatinum(IV), **B**,[29] and (*OC*-6-44)-acetato[7-(Fmoc-amino) heptanoato] diammine dichlorido platinum(IV), **C**,[93] were prepared according to established procedures. Complexes **1–3** were also obtained in their ^{15}N-labeled form by using the same synthetic procedure except for the use of $^{15}NH_3$-labeled cisplatin as the starting material (see the ESI†).[28,35,36,38]

The purity of all the compounds was routinely verified by analytical RP-HPLC (>95%, see below for the instrumental details) and elemental analysis. Elemental analyses (C, H, and N) were carried out with an EA3000 CHN Elemental Analyzer (EuroVector, Milano, Italy) and were within ±0.4% of the theoretical values.

Chromatographic analyses were performed on a Waters HPLC-MS instrument (Waters Alliance 2695 separations module) by using a C18 Phenomenex Phenosphere-NEXT column (5 μm, 250 × 4.6 mm ID). The UV-visible detector (Waters 2487 dual lambda absorbance) was set at 210 nm. The ESI-MS spectra (Waters 3100 mass detector) were recorded using the source and desolvation temperatures set to 150 and 250 °C, respectively; N_2 was used both as a drying and as a nebulizing gas. The cone and the capillary voltages were usually +30 V (positive ion mode) and 2.70 kV, respectively. The *m*/*z* values and the simulated isotope distribution patterns were used to assign the quasi-molecular ion peaks $[M + H]^+$.

The NMR spectra were measured on a Bruker Advance III NMR spectrometer operating at 500 MHz (^1H), 125.7 MHz (^{13}C) and 107.2 MHz (^{195}Pt with a spectral window of 2000 ppm). The chemical shifts in the ^1H and ^{13}C spectra were reported in parts per million (ppm) referenced to residual solvent resonances. In the ^{195}Pt NMR spectra, a solution of $K_2[PtCl_4]$ in saturated aqueous KCl was used as the external reference (δ = −1628 ppm from Na_2PtCl_6). The ^{15}N NMR spectra were referenced to a solution of $^{15}NH_4Cl$ in 1 M HCl. [^1H, ^{15}N] Heteronuclear Single Quantum Correlation (HSQC) spectra were recorded with the standard Bruker sequence hsqcetgpsiz (with 0.2 s acquisition time, 8 scans, 1.3 s relaxation delay, and 128 F_1 points) at 300 K.

Synthesis of (OC-6-44)-acetatodiamminedichlorido (4,5-dihydroxy-9,10-dioxo-9,10-dihydroanthracene-2-carboxylato)platinum(IV), 1. A mixture of **A** (0.100 g, 0.266 mmol), **rhein** (0.091 g, 0.319 mmol) and 1-[bis(dimethylamino)methylene]-1*H*-1,2,3-triazolo[4,5-*b*]pyridinium 3-oxide hexafluorophosphate (HATU, 0.145 g, 0.382 mmol) was stirred in anhydrous DMF (3 mL). The orange suspension turned deep red after the addition of 50 μL of *N*,*N*-diisopropylethylamine (DIPEA). The reaction mixture was stirred overnight in the dark at room temperature. At the end, it was centrifuged to remove unreacted **rhein**. The supernatant was transferred into a 10 mL flask and DMF was removed using a rotary evaporator (55–60 °C) to obtain an orange oil. Crude **1** was precipitated with a dichloromethane–ether mixture to give a yellow solid. This was washed with diethyl ether (four times), 1% formic acid (three times) and cold water (two times). Finally, a nitrogen flow was used to dry the solid. Yield: 0.098 g (58%). ESI-MS: *m*/*z* calcd for $C_{17}H_{17}Cl_2N_2O_8Pt$ $[M + H]^+$ 643; found, 643. ^1H NMR (DMSO-d_6) δ: 1.96 (s, 3H, CH_3), 6.66 (m, 6H, NH_3), 7.41 (d, ^3J = 8.10 Hz, 1H, H_R9), 7.74 (m, 2H, H_R11 and H_R15), 7.82 (t, 7.80 Hz, 1H, H_R10), 8.12 (s, 1H, H_R3), 11.92 (br s, 2H, OH) ppm; ^{13}C NMR (DMSO-d_6) δ: 22.6 (CH_3), 116.2 (C_R7), 117.9 (C_R3), 119.3, 119.4, 124.3 and 124.5 (C_R5, C_R11, C_R15 and C_R9), 133.3 and 133.4 (C_R12 and C_R14), 137.5 (C_R10), 140.4 (C_R2), 160.8 and 161.4 (C_R4 and C_R8), 170.8 (C_R1), 178.1 (CO_{Ac}), 181.2 (C_R13), 191.5 (C_R6) ^{195}Pt NMR (DMSO-d_6) δ: 1204 ppm.

Synthesis of the complexes

Synthesis of (*OC*-6-44)-acetatodiamminedichlorido[3-(4,5-dihydroxy-9,10-dioxo-9,10-dihydroanthracene-2-carboxamido) propanoato]platinum(IV), 2. A mixture of **B** (0.100 g, 0.224 mmol), **rhein** (0.076 g, 0.268 mmol) and HATU (0.145 g, 0.334 mmol) was stirred in anhydrous DMF (3 mL). The orange suspension turned deep red after the addition of 50 μL of *N*,*N*-diisopropylethylamine (DIPEA). The reaction mixture was stirred overnight in the dark at room temperature. At the end, it was centrifuged to remove unreacted **rhein**. The supernatant was transferred into a 10 mL flask and DMF was removed using a rotary evaporator (55–60 °C) to obtain an orange oil. Crude **2** was precipitated with a dichloromethane–ether mixture to give a yellow solid. This was washed with diethyl ether (four times), 1% formic acid (three times) and cold water (two times). Finally, a nitrogen flow was used to dry the solid. Yield: 0.059 g (37%). ESI-MS: *m*/*z* calcd for $C_{20}H_{22}Cl_2N_3O_9Pt$ $[M + H]^+$ 714; found, 714. ^1H NMR (DMSO-d_6) δ: 1.92 (s, 3H, CH_3), 2.40 (m, 2H, $H_{\beta A}2$ or $H_{\beta A}3$), 3.47 (m, 2H, $H_{\beta A}2$ or $H_{\beta A}3$), 6.53 (m, 6H, NH_3), 7.41 (d, ^3J = 8.1 Hz, 1H, H_R9), 7.75 (m, 2H, H_R11 and H_R15), 7.78 (t, ^3J = 8.1 Hz, 1H, H_R10), 8.12 (s, 1H, H_R3), 8.82 (m, 1H, NH), 11.90 (br s, 2H, OH) ppm; ^{13}C NMR (DMSO-d_6) δ: 22.9 (CH_3), 35.5 and 36.7 ($C_{\beta A}2$ and $C_{\beta A}3$), 116.1 (C_R7), 117.1, 119.4 and 122.5 (C_R3, C_R5, C_R11 and C_R15), 124.5 (C_R9), 133.4 and 133.6 (C_R12 and C_R14), 137.5 (C_R10), 141.7 (C_R2), 161.2 and 161.4 (C_R4 and C_R8), 164.1

(C_R1), 178.2 and 178.4 ($C_{\beta A}1$ and CO_{Ac}), 181.2 (C_R13), 191.5 (C_R6) ppm; ^{195}Pt NMR (DMSO-d_6) δ: 1213 ppm.

Synthesis of (*OC*-6-44)-acetatodiamminedichlorido[7-(4,5-dihydroxy-9,10-dioxo-9,10-dihydroanthracene-2-carboxamido) heptanoato]platinum(IV), 3. A mixture of **C** (0.100 g, 0.179 mmol), **rhein** (0.061 g, 0.215 mmol) and HATU (0.103 g, 0.271 mmol) was stirred in anhydrous DMF (3 mL). The orange suspension turned deep red after the addition of 50 μL of *N*,*N*-diisopropylethylamine (DIPEA). The reaction mixture was stirred overnight in the dark at room temperature. At the end, it was centrifuged to remove unreacted **rhein**. The supernatant was transferred into a 10 mL flask and DMF removed using a rotary evaporator (55–60 °C) to obtain an orange oil. Crude **3** was precipitated with a dichloromethane–ether mixture to give a yellow solid. This was washed with diethyl ether (four times), 1% formic acid (three times) and cold water (two times). Finally, a nitrogen flow was used to dry the solid. Yield: 0.0787 g (46%). ESI-MS: *m*/*z* calcd for $C_{24}H_{30}Cl_2N_3O_9Pt$ $[M + H]^+$ 770; found, 770. ^{1}H NMR (DMSO-d_6) δ: 1.31 (m, 4H, $H_{AH}4$ and $H_{AH}5$), 1.47 (m, 2H, $H_{AH}3$), 1.54 (m, 2H, $H_{AH}6$), 1.90 (s, 3H, CH_3), 2.21 (t, ^3J = 7.4 Hz, 2H, $H_{AH}2$), 2.95 (m, 2H, $H_{AH}7$ under water), 6.52 (m, 6H, NH_3), 7.41 (d, ^3J = 8.1 Hz, 1H, H_R9), 7.76 (m, 2H, H_R11 and H_R15), 7.84 (t, ^3J = 8.1 Hz, 1H, H_R10), 8.13 (s, 1H, H_R3), 11.90 (br s, 2H, OH) ppm; ^{13}C NMR (DMSO-d_6) δ: 22.9 (CH_3), 25.4, 26.3, 28.3, 28.8 ($C_{AH}3$, $C_{AH}4$, $C_{AH}5$ and $C_{AH}6$), 35.7 ($C_{AH}2$), 40.0 ($C_{AH}7$ under DMSO), 116.1 (C_R7), 117.5, 119.4 and 122.4 (C_R3, C_R5, C_R11 and C_R15), 124.5 (C_R9), 133.4 and 133.6 (C_R12 and C_R14), 137.5 (C_R10), 141.9 (C_R2), 161.2 and 161.4 (C_R4 and C_R8), 163.9 (C_R1), 178.2 (CO_{Ac}), 180.9 and 181.2 (C_R13 and $C_{AH}1$), 191.5 (C_R6) ppm; ^{195}Pt NMR (DMSO-d_6) δ: 1222 ppm.

Synthesis of the $^{15}NH_3$-labeled complexes. The syntheses of ^{15}N-labeled complexes started with the preparation of ^{15}N-cisplatin as previously reported.[35] $[PtCl_2(^{15}NH_3)_2]$ was then oxidized with H_2O_2 in acetic acid to obtain the ^{15}N-labeled monoacetato complex **$^{15}NH_3$-A**.[28] Such an intermediate was employed to prepare all the other ^{15}N-labeled complexes, as described above for **1–3**. [^{1}H, ^{15}N] HSQC spectra were recorded dissolving the complexes in DMF and diluting 20 μL of these solutions with 450 μL of Milli-Q water and 30 μL of D_2O (final [Pt] = 10 mM).

$^{15}NH_3$-1. ^{15}N NMR (50.70 MHz, DMF/D_2O/H_2O): δ −38.8 ppm (^{1}H δ = 6.59 ppm) with satellite peaks at −41.7 (^{1}H δ = 6.63 ppm) and −36.3 (^{1}H δ = 6.53 ppm) ppm ($^1J_{Pt–N}$ = 137 Hz and $^2J_{Pt–H}$ = 25 Hz). ESI-MS: *m*/*z* calcd for $C_{17}H_{17}Cl_2{}^{15}N_2O_8Pt$ $[M + H]^+$ 645; found, 645.

$^{15}NH_3$-2. ^{15}N NMR (50.70 MHz, DMF/D_2O/H_2O): δ −40.0 ppm (^{1}H δ = 6.44 ppm) with satellite peaks at −42.3 (^{1}H δ = 6.48 ppm) and −37.5 (^{1}H δ = 6.39 ppm) ppm ($^1J_{Pt–N}$ = 122 Hz and $^2J_{Pt–H}$ = 22 Hz). ESI-MS: *m*/*z* calcd for $C_{20}H_{22}Cl_2N{}^{15}N_2O_9Pt$ $[M + H]^+$ 716; found, 716.

$^{15}NH_3$-3. ^{15}N NMR (50.70 MHz, DMF/D_2O/H_2O): δ −39.7 ppm (^{1}H δ = 6.39 ppm) with satellite peaks at −42.5 (^{1}H δ = 6.44 ppm) and −37.5 (^{1}H δ = 6.34 ppm) ppm ($^1J_{Pt–N}$ = 127 Hz and $^2J_{Pt–H}$ = 25 Hz). ESI-MS: *m*/*z* calcd for $C_{24}H_{30}Cl_2N{}^{15}N_2O_9Pt$ $[M + H]^+$ 772; found 772.

Stability in solution and reduction with cytosol

Complexes **1–3** were dissolved in methanol and these solutions were diluted with complete RPMI 1640 cell culture medium (10% v/v CH_3OH; final [Pt] = 0.1 mM). The behavior in solution was monitored at 37 °C for 72 h by measuring the area of the RP-HPLC chromatographic peaks of the Pt complexes. The analyses were performed using the Waters HPLC-MS instrument described in the General procedures section (Phenomenex Phenosphere-NEXT, 250 × 4.6 mm, 5 μm C_{18} column; 70% v/v of methanol and 30% v/v of 15 mM formic acid as an eluent; flow rate was 0.5 mL min^{-1}; UV-vis detector set at 210 nm).

To simulate the intracellular reduction, the ^{15}N-labeled complexes **^{15}N-1**, **^{15}N-2**, and **^{15}N-3**, were challenged with cytosol obtained from A2780 cells by using the FractionPrep kit (BioVision, Milpitas, CA, USA). [^{1}H, ^{15}N] HSQC spectra were recorded on samples prepared as follows: the ^{15}N-labeled complexes were dissolved in 20 μL of DMF and these solutions were diluted with 450 μL of cytosol and 30 μL of D_2O (10 mM final concentration).

Cell cultures

U87-MG and T98G glioblastoma cell lines were obtained from ATCC (American Type Culture Collection, Manassas, VA, USA) and maintained in DMEM medium (Euroclone, Milan, Italy), supplemented with 10% fetal calf serum (Euroclone, Milan, Italy), 1% glutamine and 1% antibiotics mixture, 1% sodium pyruvate and 1% non-essential amino acids (both from Sigma-Aldrich, Milan, Italy) at 37 °C in a humidified 5% CO_2 atmosphere. Cells were routinely checked for *Mycoplasma* (Molecular Biology Reagent Set *Mycoplasma species*, Euroclone, UK) and all experiments were performed within 15 passages from thawing. For all the experiments, cells were exposed to TMZ, **CDDP**, **rhein** and **1–3** derivatives for 72 h. Platinum derivatives were dissolved in DMSO and immediately diluted with buffer or cell culture media prior to the treatment. The final concentration of the organic solvent never exceeded 0.1% v/v. This concentration was found to be non-toxic to the cells tested (control). For hypoxia experiments, treated cells were incubated for 24 h under normoxia and then placed into a modular incubator chamber (Billups Rothenberg Inc., Del Mar, CA, USA) flushed with a mixture of 1% O_2, 5% CO_2 and 94% N_2 at 37 °C during the last 48 h.

Growth inhibition assay

The 3-(4,5-dimethylthiazol-2-yl)-2,5-diphenyltetrazolium bromide (MTT) assay was performed on U87-MG and T98G according to previously published procedures.[94] Briefly, 3×10^3 cells were plated in each well of a 96-well plate in 0.1 mL of complete culture medium and allowed to attach for 24 h. Cells were then exposed at 37 °C for 72 h to the compounds studied at concentrations ranging between 0.05 and 300 μM. At the end of the period of incubation, MTT (0.05 mL of a 2 mg mL^{-1} stock solution in PBS) was added to each well and cells were incubated for 3 h at 37 °C. Cell supernatants were then care-

fully removed, and the blue formazan crystals formed through MTT reduction by metabolically active cells were dissolved in 0.120 mL of DMSO and the corresponding optical densities were measured at 570 nm, using an iMARK Microplate Reader (Bio-RAD). IC_{50} values were calculated based on nonlinear regression analysis of dose–response data performed with the Calcusyn software (Biosoft, Cambridge, UK). Differences between IC_{50} values were evaluated statistically by analysis of variance with Bonferroni post-test for multiple comparisons.

Scratch wound healing assay

U87-MG and T98G cells were seeded onto 6-well plates and allowed to grow approximately to confluence before a scratch was produced in cell monolayers using a 100 mL pipette tip. The scratched monolayers were then washed with fresh PBS and exposed to subtoxic concentrations of the compounds, corresponding to the respective IC_{20} concentrations, at 37 °C for 24 h. Images were acquired directly after producing the scratch and 24 h thereafter, using a camera connected to an Olympus IX81 inverted microscope.

Western blot analysis

The expression of MMP2 and MMP9 in whole cell lysates following 72 h treatment with the compounds under investigation, at concentrations corresponding to the respective IC_{20}, was detected by western blot analysis. For whole cell lysates cells were resuspended in lysis buffer (NaCl 120 mM, NaF 25 mM, EDTA 5 mM, EGTA 6 mM, sodium pyrophosphate 25 mM in tris-buffered saline TBS 20 mM pH 7.4, phenylmethanesulfonyl fluoride PMSF 2 mM, Na_3VO_4 1 mM, phenylarsine oxide 1 mM, 1% NP-40 and 10% protease inhibitor cocktail) and incubated for 10 min on ice after adding Nonidet P-40 (final concentration 0.1%) and lysates were collected by centrifugation (12 800 rpm for 20 min). The protein concentration was determined by BCA assay (Pierce, Italy) and 50 μg of protein per sample were loaded onto 8% polyacrylamide gels and separated under denaturing conditions. Protein bands were then transferred onto Hybond-P membranes (Amersham Biosciences, Italy) and western blot analysis was performed by standard techniques with mouse monoclonal antibody directed against MMP2 and MMP9 (Santa Cruz Biotechnology, Inc). Equal loading of the samples was verified by re-probing the blots with a mouse monoclonal anti-actin antibody (Santa Cruz Biotechnology, Inc.). Protein bands were visualized by G-box (Syngene, Chemi-XT4) using peroxidase-conjugated anti-mouse secondary antibodies (Sigma-Aldrich) and the Westar Supernova Substrate (Cyanagen). Densitometric analysis were performed using Image-J software and differences between obtained values were evaluated statistically by analysis of variance with Bonferroni post-test for multiple comparisons.

Ionization

The potentiometric technique was used for the determination of the pK_a values using the Pion SiriusT3 apparatus (Pion-Inc., Billerica, MA, USA). The instrument is equipped with an Ag/AgCl double junction reference pH electrode, a stirrer, a microcapillary dispenser (water, 0.5 M KOH and 0.5 M HCl), a temperature probe and a turbidity sensor. All the titration experiments were conducted at ionic strength adjusted at 0.15 M KCl either in water, cosolvent/water mixtures or in the presence of partition solvents, under a N_2 atmosphere at a controlled temperature (25 ± 0.1 °C).

In this pH-metric method, pK_a is measured by titrating a solution (obtained either by the addition of water or water/cosolvent mixtures) of the sample with an acid and a base, and the results are obtained by a complex computational process.[95] About 1 mg of the sample was weighed and put into the vial. Analyte dilution, mixing, acid/base titration, and measurement of pH were automated by the Sirius T3 measurement protocol. The pH range of the titration was from pH 12.2 to 1.8 *via* the addition of acid (0.5 M HCl) and base (0.5 M KOH), targeting 0.2 pH steps between pH measurements. Three sequential pH titrations on the same sample solution were performed.

Lipophilicity and polarity descriptors

Log D_{oct} and log D_{tol} were determined using a shake-flask procedure. A stock solution of the compound was prepared in *n*-octanol saturated with water 0.15 M KCl or toluene. 1 mL of solution was put in a separate vial to which 1 mL of buffer pH = 7.0 (ammonium acetate 10 mM) was added. All the buffers were ionic strength adjusted at 0.15 M KCl. The vial was vortexed for 10 min and the two phases were separated and analyzed by HPLC. Measurements were performed in triplicate.

The method applied for the determination of $\log k_w^{IAM}$ is already described elsewhere.[96] Briefly the analyses were performed at 30 °C with 20 mM ammonium acetate at pH 7.0 in a mixture with acetonitrile at various percentages. The stationary phase was IAM.PC.DD.2 (10 cm × 4.6 cm, 10 μm packing, 300 Å pore size) (Regis Technology, Morton Grove, IL; USA). The flow rate was 1.0 mL min^{-1}, and the injection volume was 10 mL. Chromatographic retention data at a given amount of cosolvent, expressed as $\log k^{IAM}$ (the logarithm of the retention factor), were calculated using the expression:

$$\log k^{IAM} = \log[(t_r - t_0)/t_0]$$

where t_r and t_0 are the retention times of the analyte and a non-retained compound (citric acid), respectively. All $\log k^{IAM}$ values are the average of at least three measurements. The indexes $\log k_w^{IAM}$ were calculated by an extrapolation method. Log k_w^{IAM} values were determined at least three different acetonitrile percentages (ϕ) in the mobile phases (from 10 to 40% v/v) and the intercept values of the linear relationships ($R^2 \geq 0.98$) between $\log k$ and ϕ values were assumed as $\log k_w^{IAM}$ values.

A HPLC Varian ProStar instrument equipped with a 410 autosampler with thermostable column compartment, a PDA 335 LC Detector, Galaxie Chromatography Data System Version 1.9.302.952 and CompassCDS Data System Version 4.1.0.296 was used.

$\Delta\log k_w^{IAM}$ is the difference between the logarithm of the experimental chromatographic retention factor ($\log k_w^{IAM}$) and

the value here named $\log k_w^{IAM}$ calculated using the following equation:[96]

$$c \log k_w^{IAM} = 0.92 \times BR \log D - 1.03$$

Molecular modeling

The 3D structures of the investigated Pt complexes and **rhein** were obtained using editing tools in Spartan'20 molecular modeling software (version 1.1.0, Wavefunction, Inc., Irvine, CA, USA, **https://www.wavefun.com/**). Conformational sampling was performed using Spartan'20 using Molecular Mechanics (MMFF) with default torsional angles selected by the tool. Finally, all the molecules were minimized with MOPAC2016 (version 21.237 W, Stewart Computational Chemistry, **https://openmopac.net/**). To mimic a water environment (dielectric constant ε = 80) and the interior of the membrane (dielectric constant ε = 4.81) minimization was performed applying the Conductor-like Screening Model (COSMO)[97] continuum approach implemented in MOPAC2016. The number of IMHBs was determined importing conformations in Chimera (version 1.15, UCSF, San Francisco, CA, USA, **https://www.cgl.ucsf.edu/chimera/**) and visual analysis and figures were obtained using VIDA (version 5.0.0.1, OpenEye, Santa Fe, NM, USA, **https://www.eyesopen.com/**). Finally, the IMHB plots were obtained with DataWarrior (version 5.5.0, **https://openmolecules.org/**).[98]

Conclusions

The three Pt(IV) bifunctional prodrugs based on **rhein** and **CDDP**, here designed to be tested against GBM cell lines, showed significantly better performances on U87-MG and T98G cell viability than **CDDP**. Furthermore, the effects of Pt(IV) complexes were comparable to or better than those of **rhein** on T98G and U87-MG, respectively. This last result was not unexpected, since lipophilic Pt(IV) bifunctional complexes often demonstrate a higher activity, when compared to their free metabolites (in this case, **CDDP** and **rhein**). An important result is that Pt(IV) complexes were more potent than TMZ, which represents one of the standard treatments for GBM, and retained their activity under hypoxic conditions. Hypoxia is a common feature of a solid tumor microenvironment, and it has been associated with tumor progression and resistance to chemotherapy. Therefore, it is extremely important to identify new compounds whose effects are unaffected by adaptive mechanisms activated under hypoxic conditions.

Perhaps the most interesting results in the present study concern the anti-migratory effect and the evaluation of BBB crossing of **1–3**. The migratory behavior in tumor cells of epithelial origin is a sign of invasion and metastasis and strongly indicates that the cells have undergone the transition to a mesenchymal phenotype (epithelial-to-mesenchymal transition, EMT). In this context, the presence of **rhein** (and its intracellular release after activation by reduction) in **1–3** provides Pt(IV) complexes with the ability to inhibit cancer cell migration, which is absent in **CDDP** at least at the subtoxic concentrations tested here.

CDDP is unable to cross the intact BBB, thus the limited efficacy of **CDDP**-based drugs on the CNS tumors is related to the disruption of the barrier caused by the tumor itself. As an example, in a recent paper the therapeutic activity of carmustine, cyclophosphamide and **CDDP** on intracranial Ehrlich tumor in mice was shown to be associated with the BBB permeability for these drugs (90, 20 and 8%, respectively).[99] On the other hand, in mice intracranially injected with glioma cells, **rhein** appreciably inhibited tumor progression, demonstrating its ability to cross the BBB. As far as it concerns the estimation of blood–brain barrier crossing performed here, Pt(IV) derivatives can be more prone to cross the BBB than **rhein**.

In conclusion, the conjugation between CDDP and **rhein** in a bifunctional Pt(IV) complex produced compounds in which the characteristics of the two moieties and their activity may be combined and enhanced in a sort of "intramolecular combination therapy". The results reported indicate that complexes **1–3** are worthy of further studies and that these compounds could represent an interesting improvement for GBM treatment.

Conflicts of interest

There are no conflicts to declare.

References

1 M. Weller, M. van den Bent, M. Preusser, E. Le Rhun, J. C. Tonn, G. Minniti, M. Bendszus, C. Balana, O. Chinot, L. Dirven, P. French, M. E. Hegi, A. S. Jakola, M. Platten, P. Roth, R. Ruda, S. Short, M. Smits, M. J. B. Taphoorn, A. von Deimling, M. Westphal, R. Soffietti, G. Reifenberger and W. Wick, *Nat. Rev. Clin. Oncol.*, 2021, **18**, 170–186.
2 T. F. Cloughesy, W. K. Cavenee and P. S. Mischel, in *Annual Review of Pathology: Mechanisms of Disease, Vol 9*, ed. A. K. Abbas, S. J. Galli and P. M. Howley, Annual Reviews, Palo Alto, 2014, vol. 9, pp. 1–25.
3 B. M. Alexander and T. F. Cloughesy, *J. Clin. Oncol.*, 2017, **35**, 2402–2409.
4 R. Stupp, S. Taillibert, A. Kanner, W. Read, D. M. Steinberg, B. Lhermitte, S. Toms, A. Idbaih, M. S. Ahluwalia, K. Fink, F. Di Meco, F. Lieberman, J. J. Zhu, G. Stragliotto, D. D. Tran, S. Brem, A. F. Hottinger, E. D. Kirson, G. Lavy-Shahaf, U. Weinberg, C. Y. Kim, S. H. Paek, G. Nicholas, J. Burna, H. Hirte, M. Weller, Y. Palti, M. Hegi and Z. Ram, *JAMA, J. Am. Med. Assoc.*, 2017, **318**, 2306–2316.
5 R. Batash, N. Asna, P. Schaffer, N. Francis and M. Schaffer, *Curr. Med. Chem.*, 2017, **24**, 3002–3009.
6 A. Shergalis, A. Bankhead, U. Luesakul, N. Muangsin and N. Neamati, *Pharmacol. Rev.*, 2018, **70**, 412–445.
7 H. Sun, G. W. Luo, D. H. Chen and Z. Xiang, *Front. Pharmacol.*, 2016, **7**, 16.

8 C. Wu, H. Y. Cao, H. Zhou, L. Sun, J. G. Xue, J. Y. Li, Y. Q. Bian, R. F. Sun, S. Dong, P. Liu and M. Y. Sun, *Anti-Cancer Agents Med. Chem.*, 2017, **17**, 1624–1632.
9 A. S. Tikhomirov, A. A. Shtil and A. E. Shchekotikhin, *Recent Pat. Anti-Cancer Drug Discovery*, 2018, **13**, 159–183.
10 S. Henamayee, K. Banik, B. L. Sailo, B. Shabnam, C. Harsha, S. Srilakshmi, V. G. M. Naidu, S. H. Baek, K. S. Ahn and A. B. Kunnumakkara, *Molecules*, 2020, **25**, 26.
11 E. Blacher, B. Ben Baruch, A. Levy, N. Geva, K. D. Green, S. Garneau-Tsodikova, M. Fridman and R. Stein, *Int. J. Cancer*, 2015, **136**, 1422–1433.
12 A. Levy, E. Blacher, H. Vaknine, F. E. Lund, R. Stein and L. Mayo, *Neuro-Oncology*, 2012, **14**, 1037–1049.
13 Y. Wang, X. G. Fan, T. Tang, R. Fan, C. H. Zhang, Z. B. Huang, W. J. Peng, P. P. Gan, X. G. Xiong, W. Huang and X. Huang, *Sci. Rep.*, 2016, **6**, 37098.
14 J. Chen, B. Luo, S. Wen and R. Pi, *Invest. New Drugs*, 2020, **38**, 755–764.
15 E. Gabano, M. Ravera and D. Osella, *Dalton Trans.*, 2014, **43**, 9813–9820.
16 D. Gibson, *Dalton Trans.*, 2016, **45**, 12983–12991.
17 R. G. Kenny, S. W. Chuah, A. Crawford and C. J. Marmion, *Eur. J. Inorg. Chem.*, 2017, 1596–1612.
18 D. Gibson, *J. Inorg. Biochem.*, 2019, **191**, 77–84.
19 M. Ravera, E. Gabano, M. J. McGlinchey and D. Osella, *Inorg. Chim. Acta*, 2019, **492**, 32–47.
20 D. Gibson, *J. Inorg. Biochem.*, 2021, **217**, 111353.
21 D. Gibson, *ChemMedChem*, 2021, **16**, 2188–2191.
22 B. Rangone, B. Ferrari, V. Astesana, I. Masiello, P. Veneroni, I. Zanellato, D. Osella and M. G. Bottone, *Life Sci.*, 2018, **210**, 166–176.
23 B. Ferrari, F. Urselli, M. Gilodi, S. Camuso, E. C. Priori, B. Rangone, M. Ravera, P. Veneroni, I. Zanellato, E. Roda, D. Osella and M. G. Bottone, *Neurotoxic. Res.*, 2020, **37**, 183–197.
24 B. Ferrari, E. Roda, E. C. Priori, F. De Luca, A. Facoetti, M. Ravera, F. Brandalise, C. A. Locatelli, P. Rossi and M. G. Bottone, *Front. Neurosci.*, 2021, **15**, 589906.
25 S. Raghavan, D. S. Baskin and M. A. Sharpe, *Mol. Cancer Ther.*, 2020, **19**, 2445–2453.
26 J. Jeon, S. Lee, H. Kim, H. Kang, H. Youn, S. Jo, B. Youn and H. Y. Kim, *Int. J. Mol. Sci.*, 2021, **22**, 5111.
27 M.-X. Tan, Z.-F. Wang, Q.-P. Qin, B.-Q. Zou and H. Liang, *Dalton Trans.*, 2020, **49**, 1613–1619.
28 M. Ravera, E. Gabano, I. Zanellato, F. Fregonese, G. Pelosi, J. A. Platts and D. Osella, *Dalton Trans.*, 2016, **45**, 5300–5309.
29 M. Ravera, E. Gabano, S. Tinello, I. Zanellato and D. Osella, *J. Inorg. Biochem.*, 2017, **167**, 27–35.
30 A. Kastner, I. Poetsch, J. Mayr, J. V. Burda, A. Roller, P. Heffeter, B. K. Keppler and C. R. Kowol, *Angew. Chem., Int. Ed.*, 2019, **58**, 7464–7469.
31 E. Wexselblatt, R. Raveendran, S. Salameh, A. Friedman-Ezra, E. Yavin and D. Gibson, *Chem. – Eur. J.*, 2015, **21**, 3108–3114.
32 E. Wexselblatt, E. Yavin and D. Gibson, *Angew. Chem., Int. Ed.*, 2013, **52**, 6059–6062.
33 E. Gabano, B. Rangone, E. Perin, G. Caron, G. Ermondi, M. Vallaro, V. Gandin, C. Marzano, A. Barbanente, N. Margiotta and M. Ravera, *Dalton Trans.*, 2021, **50**, 4663–4672.
34 M. Ravera, E. Gabano, I. Zanellato, B. Rangone, E. Perin, B. Ferrari, M. G. Bottone and D. Osella, *Dalton Trans.*, 2021, **50**, 3161–3177.
35 M. S. Davies, M. D. Hall, S. J. Berners-Price and T. W. Hambley, *Inorg. Chem.*, 2008, **47**, 7673–7680.
36 E. Wexselblatt and D. Gibson, *J. Inorg. Biochem.*, 2012, **117**, 220–229.
37 D. Gibson, *Dalton Trans.*, 2009, 10681–10689.
38 A. Nemirovski, Y. Kasherman, Y. Tzaraf and D. Gibson, *J. Med. Chem.*, 2007, **50**, 5554–5556.
39 E. Gabano, M. Ravera, F. Trivero, S. Tinello, A. Gallina, I. Zanellato, M. B. Gariboldi, E. Monti and D. Osella, *Dalton Trans.*, 2018, **47**, 8268–8282.
40 S. Kohsaka, L. Wang, K. Yachi, R. Mahabir, T. Narita, T. Itoh, M. Tanino, T. Kimura, H. Nishihara and S. Tanaka, *Mol. Cancer Ther.*, 2012, **11**, 1289–1299.
41 R. R. Wallace-Brodeur and S. W. Lowe, *Cell. Mol. Life Sci.*, 1999, **55**, 64–75.
42 Z. H. Siddik, *Oncogene*, 2003, **22**, 7265–7279.
43 K. Bajbouj, C. Mawrin, R. Hartig, J. Schulze-Luehrmann, A. Wilisch-Neumann, A. Roessner and R. Schneider-Stock, *J. Neuro-Oncol.*, 2012, **107**, 503–516.
44 C. M. Park, M. J. Park, H. J. Kwak, S. I. Moon, D. H. Yoo, H. C. Lee, I. C. Park, C. H. Rhee and S. I. Hong, *Int. J. Oncol.*, 2006, **28**, 119–125.
45 G. P. Dunn, M. L. Rinne, J. Wykosky, G. Genovese, S. N. Quayle, I. F. Dunn, P. K. Agarwalla, M. G. Chheda, B. Campos, A. Wang, C. Brennan, K. L. Ligon, F. Furnari, W. K. Cavenee, R. A. Depinho, L. Chin and W. C. Hahn, *Genes Dev.*, 2012, **26**, 756–784.
46 V. A. Cuddapah, S. Robel, S. Watkins and H. Sontheimer, *Nat. Rev. Neurosci.*, 2014, **15**, 455–465.
47 T. T. Lah, M. Novak and B. Breznik, *Semin. Cancer Biol.*, 2020, **60**, 262–273.
48 D. R. Welch and D. R. Hurst, *Cancer Res.*, 2019, **79**, 3011–3027.
49 C. C. Liang, A. Y. Park and J. L. Guan, *Nat. Protoc.*, 2007, **2**, 329–333.
50 E. Monti, E. Marras, P. Prini and M. B. Gariboldi, *Eur. J. Pharmacol.*, 2020, **881**, 173210.
51 J. Luo, X. Luo, X. Liu, Z. Q. Fang, J. Xu and L. K. Li, *OncoTargets Ther.*, 2020, **13**, 1321–1330.
52 Y. Chen, *Bio-Protoc.*, 2012, **2**, e100.
53 B. X. Yu, L. Zou, S. Li and Y. L. Du, *Eur. Rev. Med. Pharmacol. Sci.*, 2019, **23**, 8456–8467.
54 J. Zhang and J. Y. Fan, *Exp. Ther. Med.*, 2020, **20**, 1145–1152.
55 I. Emanuelsson, K. Wikvall, T. Friman and M. Norlin, *Basic Clin. Pharmacol. Toxicol.*, 2018, **123**, 130–136.
56 P. Yin, G. Z. Song and Z. H. Jiang, *Cancer Chemother. Pharmacol.*, 2018, **81**, 863–872.
57 M. L. Lin, J. G. Chung, Y. C. Lu, C. Y. Yang and S. S. Chen, *Oral Oncol.*, 2009, **45**, 531–537.

58 B. Y. Ren, W. J. Guo, Y. W. Tang, J. Zhang, N. Xiao, L. Zhang and W. L. Li, *Biol. Pharm. Bull.*, 2019, **42**, 568–572.
59 J. A. Eble and S. Niland, *Clin. Exp. Metastasis*, 2019, **36**, 171–198.
60 H. C. Zheng, H. Takahashi, Y. Murai, Z. G. Cui, K. Nomoto, H. Niwa, K. Tsuneyama and Y. Takano, *Anticancer Res.*, 2006, **26**, 3579–3583.
61 F. Q. Wang, J. So, S. Reierstad and D. A. Fishman, *Int. J. Cancer*, 2005, **114**, 19–31.
62 M. Nakada, Y. Okada and J. Yamashita, *Front. Biosci.*, 2003, **8**, E261–E269.
63 G. M. Zhou, F. H. Peng, Y. P. Zhong, Y. H. Chen, M. Tang and D. R. Li, *Int. J. Oncol.*, 2017, **50**, 933–941.
64 T. M. Yeung, S. C. Gandhi and W. F. Bodmer, *Proc. Natl. Acad. Sci. U. S. A.*, 2011, **108**, 4382–4387.
65 J. T. de Oliveira, C. Ribeiro, R. Barros, C. Gomes, A. J. de Matos, C. A. Reis, G. R. Rutteman and F. Gartner, *PLoS One*, 2015, **10**, e0134458.
66 L. Schito and G. L. Semenza, *Trends Cancer*, 2016, **2**, 758–770.
67 G. L. Semenza, *Oncogene*, 2010, **29**, 625–634.
68 G. L. Semenza, *Cell*, 2012, **148**, 399–408.
69 D. A. Cavazos and A. J. Brenner, *Neurobiol. Dis.*, 2016, **85**, 227–233.
70 C. A. Waker and R. M. Lober, in *Myelin: Basic and Clinical Advances*, ed. K. Sango, J. Yamauchi, T. Ogata and K. Susuki, Springer, Singapore, 2019, vol. 1190, pp. 281–297.
71 A. M. Shannon, D. J. Bouchier-Hayes, C. M. Condron and D. Toomey, *Cancer Treat. Rev.*, 2003, **29**, 297–307.
72 P. Vaupel and A. Mayer, *Cancer Metastasis Rev.*, 2007, **26**, 225–239.
73 N. Devarajan, R. Manjunathan and S. K. Ganesan, *Crit. Rev. Oncol. Hematol.*, 2021, **162**, 103327.
74 S. Karmakar, S. Chatterjee, K. Purkait and A. Mukherjee, *Dalton Trans.*, 2016, **45**, 11710–11722.
75 Z. C. Xu, J. Zhao, S. H. Gou and G. Xu, *Chem. Commun.*, 2017, **53**, 3749–3752.
76 Z. Wang, Z. Deng and G. Zhu, *Dalton Trans.*, 2019, **48**, 2536–2544.
77 H. R. Mellor, S. Snelling, M. D. Hall, S. Modok, M. Jaffar, T. W. Hambley and R. Callaghan, *Biochem. Pharmacol.*, 2005, **70**, 1137–1146.
78 E. Schreiber-Brynzak, V. Pichler, P. Heffeter, B. Hanson, S. Theiner, I. Lichtscheidl-Schultz, C. Kornauth, L. Bamonti, V. Dhery, D. Groza, D. Berry, W. Berger, M. Galanski, M. A. Jakupec and B. K. Keppler, *Metallomics*, 2016, **8**, 422–433.
79 S. Goschl, E. Schreiber-Brynzak, V. Pichler, K. Cseh, P. Heffeter, U. Jungwirth, M. A. Jakupec, W. Berger and B. K. Keppler, *Metallomics*, 2017, **9**, 309–322.
80 O. van Tellingen, B. Yetkin-Arik, M. C. de Gooijer, P. Wesseling, T. Wurdinger and H. E. de Vries, *Drug Resist. Updates*, 2015, **19**, 1–12.
81 C. D. Arvanitis, G. B. Ferraro and R. K. Jain, *Nat. Rev. Cancer*, 2020, **20**, 26–41.
82 H. van de Waterbeemd, G. Camenisch, G. Folkers, J. R. Chretien and O. A. Raevsky, *J. Drug Targeting*, 1998, **6**, 151–165.
83 C. Pidgeon, S. W. Ong, H. L. Liu, X. X. Qiu, M. Pidgeon, A. H. Dantzig, J. Munroe, W. J. Hornback, J. S. Kasher, L. Glunz and T. Szczerba, *J. Med. Chem.*, 1995, **38**, 590–594.
84 R. C. Young, R. C. Mitchell, T. H. Brown, C. R. Ganellin, R. Griffiths, M. Jones, K. K. Rana, D. Saunders and I. R. Smith, *J. Med. Chem.*, 1988, **31**, 656–671.
85 B. Testa, P.-A. Carrupt, P. Gaillard and R.-S. Tsai, in *Lipophilicity in Drug Action and Toxicology*, ed. V. Pliška, B. Testa and H. van de Waterbeemd, VCH, Weinheim, Germany, 1996, ch. 4, pp. 49–71.
86 R. A. Conradi, P. S. Burton and R. T. Borchardt, in *Lipophilicity in Drug Action and Toxicology*, ed. V. Pliška, B. Testa and H. van de Waterbeemd, VCH, Weinheim, Germany, 1996, ch. 14, pp. 233–252.
87 G. Ermondi, M. Vallaro and G. Caron, *Drug Discovery Today*, 2020, **25**, 1585–1591.
88 L. Grumetto, C. Carpentiero and F. Barbato, *Eur. J. Pharm. Sci.*, 2012, **45**, 685–692.
89 L. Grumetto, C. Carpentiero, P. Di Vaio, F. Frecentese and F. Barbato, *J. Pharm. Biomed. Anal.*, 2013, **75**, 165–172.
90 M. Shalaeva, G. Caron, Y. A. Abramov, T. N. O'Connell, M. S. Plummer, G. Yalamanchi, K. A. Farley, G. H. Goetz, L. Philippe and M. J. Shapiro, *J. Med. Chem.*, 2013, **56**, 4870–4879.
91 S. C. Dhara, *Indian J. Chem.*, 1970, **8**, 193–194.
92 G. Pelosi, M. Ravera, E. Gabano, F. Fregonese and D. Osella, *Chem. Commun.*, 2015, **51**, 8051–8053.
93 E. Gabano, G. Pinton, C. Balzano, S. Boumya, D. Osella, L. Moro and M. Ravera, *Molecules*, 2021, **26**, 4740.
94 M. B. Gariboldi, E. Taiana, M. C. Bonzi, I. Craparotta, S. Giovannardi, M. Mancini and E. Monti, *Cancer Lett.*, 2015, **364**, 156–164.
95 A. Avdeef, K. J. Box, J. E. A. Comer, M. Gilges, M. Hadley, C. Hibbert, W. Patterson and K. Y. Tam, *J. Pharm. Biomed. Anal.*, 1999, **20**, 631–641.
96 G. Ermondi, M. Vallaro and G. Caron, *Eur. J. Pharm. Sci.*, 2018, **114**, 385–390.
97 A. Klamt and G. Schuurmann, *J. Chem. Soc., Perkin Trans. 2*, 1993, 799–805.
98 T. Sander, J. Freyss, M. von Korff and C. Rufener, *J. Chem. Inf. Model.*, 2015, **55**, 460–473.
99 A. N. Stukov, V. G. Bespalov, V. A. Alexandrov, A. L. Semenov, G. S. Kireeva, T. Y. Semiglazova, L. V. Filatova and D. A. Baranenko, *Drug Res.*, 2020, **70**, 86–90.